# Criticality and mechanical enhancement in composite fiber networks

Jan Maarten van Doorn, Luuk Lageschaar, Joris Sprakel, and Jasper van der Gucht*
*Physical Chemistry and Soft Matter, Wageningen University, Stippeneng 4, 6708 WE, Wageningen, The Netherlands*
(Received 9 November 2016; published 21 April 2017)

Many biological materials consist of sparse networks of disordered fibers, embedded in a soft elastic matrix. The interplay between rigid and soft elements in such composite networks leads to mechanical properties that can go far beyond the sum of those of the constituents. Here we present lattice-based simulations to unravel the microscopic origins of this mechanical synergy. We show that the competition between fiber stretching and bending and elastic deformations of the matrix gives rise to distinct mechanical regimes, with phase transitions between them that are characterized by critical behavior and diverging strain fluctuations and with different mechanisms leading to mechanical enhancement.

DOI: 10.1103/PhysRevE.95.042503

## I. INTRODUCTION

Many materials, ranging from textiles and paper to connective tissue and the cytoskeleton of living cells, have a microscopic structure that consists of crosslinked fibers. Theoretical progress in the last decades has led to a detailed understanding of the physics of such fiber networks [1]. Because stiff fibers resist not only stretching, but also bending, the mechanical behavior of fiber networks differs significantly from that of networks of flexible polymers. Different mechanical regimes can be observed: at high densities fiber networks deform affinely and the elasticity is governed by fiber stretching, while at lower densities there is a crossover to a nonaffine, bending-dominated regime [2–6].

Although experiments on model networks give support to the existence of different mechanical regimes [7–9], the current theories fall short in describing real biomaterials. An important reason for this is that natural materials are almost without exception composite materials that consist of mixtures of elements of different rigidity: the cytoskeleton is a complex network of (partially bundled) actin filaments, intermediate filaments, and microtubules [10]; the extracellular matrix consists of stiff collagen fibers in a matrix of more flexible polymers [11]; and also many synthetic high-performance materials are composites of soft and rigid fibers [12–16]. Recent experimental work has shown that networks of stiff fibers embedded in an elastic matrix can have an elastic modulus that significantly exceeds the sum of the moduli of the two individual networks [17,18]. It was hypothesized that this mechanical enhancement was caused by a suppression of nonaffine deformation modes in the rigid fiber network due to the reaction forces in the softer network. However, a theoretical underpinning of this hypothesis was missing. Previous models considered the effect of sparse rigid inclusions in a softer base network [19–24]. These models indeed showed that the interplay between stiff and soft components can strongly affect the deformation modes and stiffness of a composite network. However, there has been no systematic investigation of how the mechanical response of a composite network depends on the connectivity of the fiber network and on the stiffness of the individual constituents. Here, we present a model that allows us to explore the mechanics of composite networks over a large range of parameters and compositions, both for sparse fiber networks and for highly connected fibers.

## II. MODEL

We use numerical simulations to study the mechanics of disordered composite networks, consisting of crosslinked fibers embedded in a soft elastic matrix. Both the fibers and the polymers that constitute the background matrix are arranged on a two-dimensional (2D) triangular lattice with lattice spacing $l_0$, as shown in Fig. 1. The effects of connectivity are explored by randomly removing segments of the fiber network with a probability $1-p$, so that the average connectivity equals $z = 6p$. Sequences of contiguous colinear fiber segments are treated as elastic rods, characterized by a stretch modulus $\mu_1$ and a bending modulus $\kappa_1$. Since fibers in biomaterials are typically much softer with respect to bending than to stretching [1], we will only consider the case that $\kappa_1 \ll \mu_1 l_0^2$. Intersecting fibers are assumed to be crosslinked with permanent but freely hinged bonds. The background matrix is modelled as a homogeneous network of undiluted central force springs with stretch modulus $\mu_2$. The two networks are linked to each other at each vertex of the lattice. To investigate the mechanical response of the composite network, we calculate the linear shear modulus $G$ by applying a shear strain $\gamma = 10^{-2}$ to the network by translating the horizontal boundaries to which the fibers and springs are attached. The network is then relaxed by minimizing the total mechanical energy

$$E = \frac{1}{2}\frac{\mu_1}{l_0}\sum_{\langle ij\rangle} g_{ij}^{(1)}(\Delta l_{ij})^2 + \frac{1}{2}\frac{\kappa_1}{l_0^3}\sum_{\langle ijk\rangle} g_{ij}^{(1)} g_{jk}^{(1)}(\Delta\theta_{ijk})^2 + \frac{1}{2}\frac{\mu_2}{l_0}\sum_{\langle ij\rangle}(\Delta l_{ij})^2, \quad (1)$$

where $l_0$ is the lattice spacing, $\Delta l_{ij}$ the extension of the segment between vertices $i$ and $j$, $\Delta\theta_{ijk}$ the angle between neighboring bonds $i$–$j$ and $j$–$k$, and $g_{ij}^{(1)} = 1$ if there is a fiber segment between vertices $i$ and $j$, while $g_{ij}^{(1)} = 0$ otherwise. The first term represents the stretch energy of the fibers, the second term the bending energy, and the third term the elastic energy of the matrix. The first and third summations extend over all bonds $i$–$j$, while the second summation extends only over colinear

*jasper.vandergucht@wur.nl

 

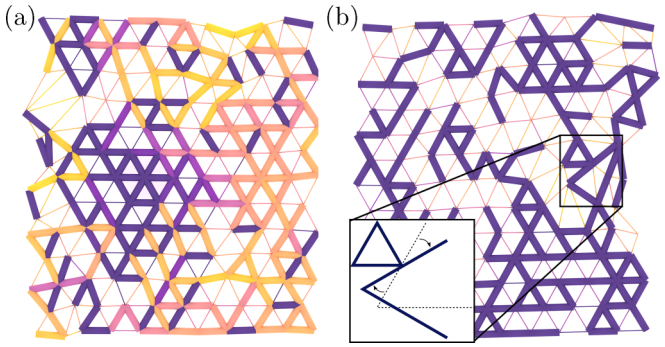


FIG. 1. Composite networks on a triangular lattice. A small section of a deformed network of fibers in a soft matrix, with $\kappa_1/(\mu_2 l_0^2) = 10^{-6}$ and $\mu_2/\mu_1 = 10^{-12}$ for (a) $p = 0.65$ and (b) $p = 0.45$. Thick segments represent fiber segments, color-coded for their bending energy (yellow: strongly bent, blue: weakly bent), and thin segments represent the background matrix, color-coded for stretching energy (yellow: strongly stretched; blue: weakly stretched). Inset in (b) shows an example of a rigid rotation of a fiber cluster.

neighboring bonds. This energy can be expressed in terms of the node displacements [6] using $\Delta l_{ij} = (\mathbf{u}_j - \mathbf{u}_i) \cdot \hat{\mathbf{r}}_{ij}$ with $\hat{\mathbf{r}}_{ij}$ the unit vector along the $i$–$j$ bond, and $\Delta\theta_{ijk} = (\mathbf{u}_k + \mathbf{u}_i - 2\mathbf{u}_j) \times \hat{\mathbf{r}}_{ij}$. The energy is minimized using lower upper (LU) decomposition, giving the equilibrium nodal displacements. The shear modulus is calculated as $G = (2/A)(E/\gamma^2)$ where $A$ is the area of the network. In our simulations we use $A = 4 \times 10^4 l_0^2$. Results for other system sizes are shown in Fig. 7 in Appendix B.

## III. RESULTS

### A. Mechanical regimes

In Fig. 2, we show the shear modulus as a function of the connectivity $p$ for various values of the matrix stiffness $\mu_2$. For $\mu_2 = 0$, $G$ vanishes when the connectivity is lower than a critical rigidity threshold. For fibers with no bending rigidity ($\kappa_1 = 0$, dashed line), this threshold is $p_{\rm cf} \approx 0.651$, as given by Maxwell's criterion for isostatic networks of central force

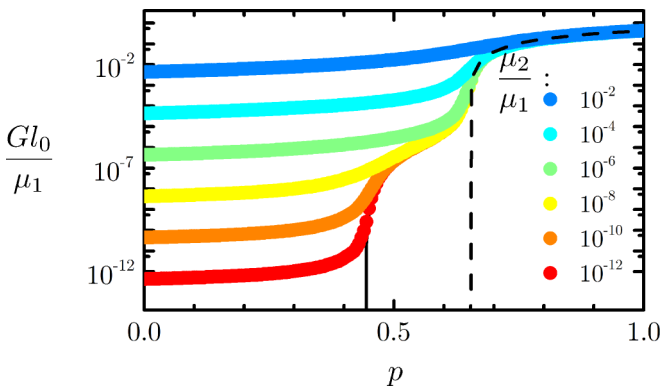


FIG. 2. Elasticity of composite networks. Shear modulus $G$ (in units $\mu_1/l_0$) as a function of the bond probability $p$ for $\kappa_1/\mu_1 l_0^2 = 10^{-6}$ and for a range of stiffnesses of the background matrix. The black line corresponds to $\mu_2 = 0$ and the dashed line to $\mu_2 = 0$ and $\kappa_1 = 0$.

springs [25]. For nonzero $\kappa_1$, however, the rigidity threshold shifts discontinuously to a lower value, $p_b \approx 0.442$, which is independent of $\kappa_1$ for $\kappa_1 > 0$ (black line). The results for different values of the bending rigidity are shown in Fig. 6 in Appendix A. In the presence of an elastic matrix with nonzero stretch modulus $\mu_2$, the network is mechanically stable for any value of $p$. However, features of the mechanical transitions at $p_{\rm cf}$ and $p_b$ can still be seen, as the shear modulus decreases very steeply with decreasing $p$ around these points (Fig. 2). This suggests that both points mark a transition between distinct mechanical regimes in the composite network.

To investigate the nature of these different regimes, we examine both crossover regions in more detail. For low values of $\mu_2$, the mechanical response of the composite network is dominated by the fiber network for $p$ sufficiently above $p_b$. We therefore expect that the crossover region at $p_{\rm cf}$ is similar to the one observed in single-component fiber networks. As shown previously [6], in such networks the central force threshold coincides with a transition from a stretching-dominated regime for $p > p_{\rm cf}$ to a bending-dominated regime for $p < p_{\rm cf}$. The presence of an elastic matrix as embedding medium is expected to affect this transition because fiber bending is a nonaffine deformation mode, which inevitably leads to additional strain in the medium. The elastic energy stored in the matrix due to the bending of an embedded fiber increases proportionally to the matrix stiffness $\mu_2$ [27]. We therefore expect the resistance to bending to increase linearly with $\mu_2$. Indeed, we find that we can collapse our data by introducing an effective bending rigidity, which is the sum of the intrinsic bending rigidity and a matrix-induced bending resistance (see Appendix C)

$$\kappa_{\rm eff} = \kappa_1 + \mu_2 l_0^2. \tag{2}$$

This is shown in Fig. 3(a), where we plot the scaling form

$$G = \frac{\mu_1}{l_0} |\Delta p_{\rm cf}|^{\beta} \mathcal{G}_{\pm}^{\rm cf}\left(\frac{\kappa_{\rm eff}}{\mu_1 l_0^2} |\Delta p_{\rm cf}|^{-\alpha}\right) \tag{3}$$

with $\Delta p_{\rm cf} = p - p_{\rm cf}$ and with scaling exponents $\alpha = 3.0$ and $\beta = 1.4$, in agreement with previous findings [6]. The universal scaling function $\mathcal{G}_{\pm}^{\rm cf}(x)$ consists of three branches that characterize three different mechanical regimes. For $x \ll 1$, $\mathcal{G}_{+}^{\rm cf}(x) \sim$ const. and $\mathcal{G}_{-}^{\rm cf}(x) \sim x$. This implies a stretching-dominated regime with $G \sim \mu_1 |\Delta p_{\rm cf}|^{\beta}$ above the transition ($\Delta p_{\rm cf} > 0$), and a bending-dominated regime with $G \sim \kappa_{\rm eff} |\Delta p_{\rm cf}|^{\beta-\alpha}$ below the transition ($\Delta p_{\rm cf} < 0$). In the bending-dominated regime, the shear modulus is governed by the effective bending resistance of the fibers [Eq. (2)]: for very soft matrices ($\mu_2 < \kappa_1 l_0^{-2}$) the response is dominated by the intrinsic bending rigidity of the fibers, $G \sim \kappa_1$, while for stiffer matrices ($\mu_2 > \kappa_1 l_0^{-2}$) the shear modulus is determined by the induced bending rigidity due to the matrix: $G \sim \mu_2$. Very close to the critical threshold, we find a crossover regime with anomalous scaling [6] $G \sim \kappa_{\rm eff}^{\beta/\alpha} \mu_1^{1-\beta/\alpha}$ independent of $\Delta p_{\rm cf}$, as observed from the critical branch in Fig. 3(a).

At $p = p_b$ there is a second transition, now from a bending-dominated regime to a matrix-dominated regime. Again, we can capture the different regimes around this transition by a scaling form

$$G = \frac{\kappa_1}{l_0^3} |\Delta p_b|^{\delta} \mathcal{G}_{\pm}^{b}\left(\frac{\mu_2 l_0^2}{\kappa_1} |\Delta p_b|^{-\gamma}\right) \tag{4}$$

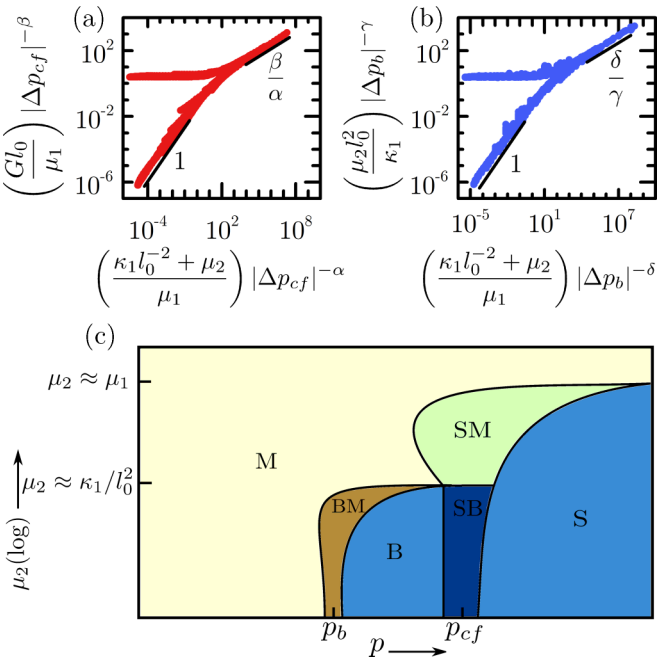


FIG. 3. Mechanical regimes in composite networks. Scaling analysis of the shear modulus in the vicinity of (a) the central force isostatic point $p_{cf}$ and (b) the rigidity threshold $p_b$, for a wide variety of values of $\kappa_1$ and $\mu_2$. Values of the critical exponents: $\alpha = 3.0$, $\beta = 1.4$, $\gamma = 4.5$, $\delta = 3.0$. (c) Mechanical phase diagram of composite networks: S: stretching-dominated ($G \sim \mu_1$), B: bending-dominated ($G \sim \kappa_1$), M: matrix-dominated ($G \sim \mu_2$), SB: stretch-bend coupled ($G \sim \mu_1^{1-x}\kappa_1^x$), SM: stretch-matrix coupled ($G \sim \mu_1^{1-x}\mu_2^x$), BM: bend-matrix coupled ($G \sim \kappa_1^{1-y}\mu_2^y$).

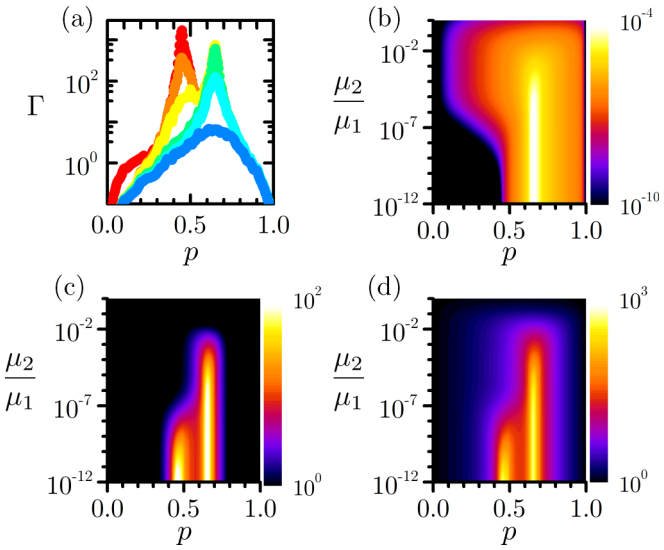


FIG. 4. Nonaffine deformations in composite networks. (a) Nonaffinity as a function of connectivity $p$ for several values of $\mu_2$ (same color coding as in Fig. 2). (b) Bending energy per unit area and unit strain, $E_b/A\gamma^2$, as a function of $p$ and $\mu_2$. (c) Rigid body rotations: mean-squared rotation angle of the end-to-end vector of fibers, averaged over all fibers in the network $\langle \Delta\phi^2 \rangle$, compared to that for the affinely deformed network as a function of $p$ and $\mu_2$. (d) Relative deformation energy of the background matrix, compared to the affinely deformed network, $E_2/E_2^{(\mathrm{aff})}$, as a function of $p$ and $\mu_2$. The bending rigidity $\kappa_1 = 10^{-6}\mu_2 l_0^2$ in all cases.

with $\Delta p_b = p - p_b$ and $\mathcal{G}_{\pm}^b(x)$ another universal scaling function. The data are found to collapse with critical exponents $\gamma = 4.5$ and $\delta = 3.0$. Again, we see three branches, corresponding to three different mechanical regimes. Above the transition for $x \ll 1$ we find $\mathcal{G}_+^b(x) \sim$ const and $G \sim \kappa_1 |\Delta p_b|^\delta$, which corresponds to the rigidity percolation scaling of a bending-dominated network [6]. Below the transition, for $x \ll 1$ we find $\mathcal{G}_-^b(x) \sim x$ and $G \sim \mu_2 |\Delta p_b|^{\delta-\gamma}$. In this regime the fiber network is below its rigidity threshold, and the composite network consists of an elastic matrix with embedded, nonpercolating fiber clusters. Indeed, the scaling that we find is very similar to the one found for a central force network with rigid inclusions [28,29]. Very close to the transition we again find an anomalous scaling regime in which the modulus becomes independent of $\Delta p_b$ and is governed by both bending and matrix contributions, with $G \sim \kappa_1^{1-\delta/\gamma}\mu_2^{\delta/\gamma}$. The different mechanical regimes that we find for our composite network are summarized in the phase diagram in Fig. 3(c), which clearly highlights the rich behavior of composite networks.

It is well established that the mechanics of weakly connected disordered networks are governed by nonaffine deformation modes [1–6]. This raises the question whether the different mechanical regimes that we observe originate from a transition between different nonaffine modes. We examine the the nonaffine fluctuations by calculating the mean-square deviation from a uniform, affine strain field [30]

$$\Gamma = \frac{1}{\gamma^2 l_0^2} \langle (\mathbf{u} - \mathbf{u}^{(\mathrm{aff})})^2 \rangle. \tag{5}$$

Here $\mathbf{u}$ and $\mathbf{u}^{(\mathrm{aff})}$ are the actual displacement and the affine displacement of a node, respectively. We find a strong, cusp-like increase of the nonaffine fluctuations in the vicinity of both $p_{\mathrm{cf}}$ and $p_b$, highlighting the critical state of the fiber network at these points [Fig. 4(a)]. From Fig. 1 it is clear, however, that the nature of the nonaffine modes is very different in these two regimes. For $p \approx p_{\mathrm{cf}}$, the deformation field is characterized by large and heterogeneous bending fluctuations [Figs. 1(a) and 4(b)]. This is in agreement with earlier work [2–6], where the central force threshold was shown to mark a transition from an affine, stretching-dominated regime for $p > p_{\mathrm{cf}}$ to a nonaffine, bending-dominated regime for $p < p_{\mathrm{cf}}$. By contrast, the increase in $\Gamma$ at $p \approx p_b$ is not associated with bending fluctuations [Fig. 1(b)], but can be ascribed to rigid body motions of fibers or fiber clusters [insets of Figs. 1(b) and 4(c)] that become more and more prominent as the connectivity of the network decreases. At the rigidity threshold $p_b$, the fiber network becomes floppy and all the strain can be accommodated by such rigid body motions without elastic energy cost in the fiber network [6,26,31]. However, while the nonaffine modes are soft modes for the fiber network, they lead to additional deformations in the background matrix, so that the elastic energy of the matrix is strongly increased in regions where the nonaffine fluctuations are large [Fig. 4(d)]. This means that the final deformation field in a composite network is a compromise between energy stored in the fiber network

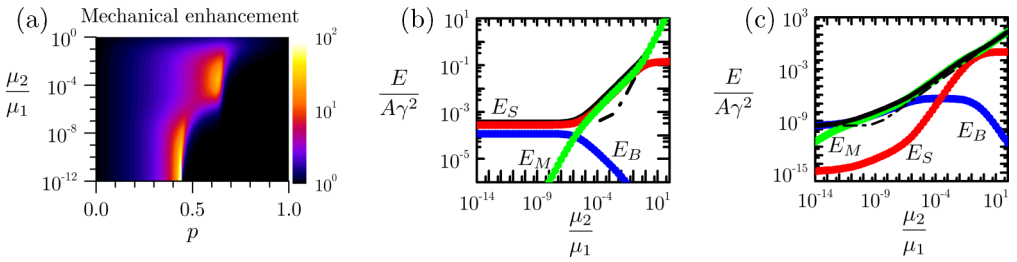


FIG. 5. Mechanical enhancement in composites. (a) Enhancement of the shear modulus with respect to the summed moduli of the individual networks, $G/(G_1 + G_2)$ as a function of $p$ and $\mu_2$ for $\kappa_1 = 10^{-6}\mu_2 l_0^2$. (b,c) Different energy contributions to the shear modulus [$E_b$ (blue): fiber bending; $E_s$ (red): fiber stretching; $E_m$ (green): matrix deformation] as a function of $\mu_2$ for (b) $p = 0.65$ and (c) $p = 0.45$. The black line gives the total elastic energy and the dashed line the sum of the energies of the separate networks, so that the difference between the solid and the dashed line represents the mechanical enhancement.

(which can be reduced by nonaffine modes) and energy stored in the matrix (which is enhanced by nonaffine deformations). As the matrix becomes stiffer, the nonaffine fluctuations are increasingly suppressed (Fig. 4). The scaling of the nonaffine fluctuations with $\mu_2$ and $\kappa_1$ is discussed in Appendix B (Fig. 7).

### B. Mechanical enhancement

The main reason for the interest in composite materials is that the interplay between the different components can lead to highly synergistic properties, such as enhanced strength and rigidity [12–18]. We therefore consider the enhancement of the modulus of the composite network in comparison to the sum of the moduli of the individual networks [Fig. 5(a)]. The highest enhancement, with a modulus that exceeds those of the individual networks by up to a factor $10^2$, is observed in the two crossover regions labeled SM and BM in Fig. 3(c). We can understand the origin of the enhancement in these regimes by considering the different contributions to the modulus. At $p \approx p_{cf}$ [Fig. 5(b)], the modulus is dominated by bending contributions for small $\mu_2$. These bending modes are suppressed by the elastic matrix when $\mu_2$ increases [Fig. 4(b)], leading to a more affine deformation. However, this goes at the cost of increased fiber stretching, and this increase in stretching energy stiffens the network. As discussed above, at $p \approx p_b$, the deformation of the fiber network is characterized by floppy modes, in which large clusters of fibers undergo rigid body motions without being strained. As the matrix becomes stiffer, these rigid body motions are suppressed at the cost of increased fiber bending [Figs. 4(b) and 4(c)]. Thus, while the enhancement around $p_{cf}$ is caused by the suppression of bending modes, the enhancement around $p_b$ is associated with an increase in fiber bending [Fig. 5(c)].

## IV. DISCUSSION

We reveal a very rich mechanical behavior of composite networks. Small variations in composition can lead to large differences in mechanical response. This may be an important reason why composite structures are so abundant in biology, where adaptiveness is often crucial. Indeed, it has been argued that many biological networks have a connectivity in the vicinity of a critical regime [9], where they are most susceptible to small changes. Our results show that these are also the regions where mechanical synergy is to be expected. As Fig. 5(a) shows, a nontrivial crosstalk between the two networks occurs only for specific compositions and stiffness ratios between the two networks. For densely crosslinked fiber networks ($p > p_{cf}$), where the mechanics of the fiber network is dominated by affine stretching modes even in the absence of an elastic matrix, there is no enhancement. However, for bending-dominated fiber networks ($p_b < p < p_{cf}$), there is a significant range of matrix stiffnesses where strong enhancement is expected to occur. Recent experiments report the modulus of a mixture of two protein fiber networks with varying composition [17]. The network of the stiffest fibers was kept constant, while the stiffness of the soft background matrix was varied over a large range. A significant mechanical enhancement was found over approximately six decades in modulus of the soft network, with a maximum enhancement factor of approximately 3 with respect to the sum of the moduli of the separate networks. These experiments correspond to a vertical cross-section in Fig. 5(a), i.e., a variation in $\mu_1$ at constant connectivity of the stiff network $p$. Even though the precise value of $p$ is not known for the experimental system, it presumably lies between $p_b$ and $p_{cf}$ since the network was argued to be in the bending-dominated regime. As shown in Fig. 5(a), our model also predicts a modulus enhancement in this regime over a range spanning approximately six decades in $\mu_1$. The maximum enhancement of 3 found in the experiment suggests that the network is significantly below $p_{cf}$, and that an even stronger enhancement may be obtained for $p$ values closer to the central force threshold.

While our focus has been on linear elasticity, we expect that also the nonlinear response of composite networks will differ greatly from that of single-component networks. Fiber networks are known to become stiffer as the strain increases [7] due to a transition from bending to stretching-dominated elasticity [32]. Recent experiments have shown that this strain stiffening can be suppressed completely when the fibers are embedded in a soft elastic matrix [17]. Our results suggest that this may be the result of a suppression of bending modes already in the linear regime. Finally, the suppression of nonaffine fluctuations by the background matrix leads to a more homogeneous stress distribution in the network. This should have large consequences for the nucleation and propagation of cracks in the material, and may thus contribute to the large increase in fracture strength found in double network hydrogels [15,16].

## ACKNOWLEDGMENTS

This work is part of the Industrial Partnership Programme Hybrid Soft Materials that is carried out under an agreement between Unilever Research and Development B.V. and the Netherlands Organisation for Scientific Research (NWO) and of the project SOFTBREAK funded by the European Research Council (ERC Consolidator Grant).


## APPENDIX A: EFFECT OF THE FIBER BENDING RIGIDITY

To investigate the effect of the fiber bending rigidity on the shear modulus of composite networks, we repeat the calculations of Fig. 2 for different values of $\kappa_1$. The results are shown in Fig. 6. For $\kappa_1 = 0$, the single fiber network becomes unstable at the central force isostatic threshold $p_{cf} = 0.651$ [Fig. 6(a)]. For this case, our simulations of composite networks are identical to previous findings for the so-called superelastic problem [29], consisting of central force spring networks, where a fraction $p$ of the bonds have a stretch modulus $\mu_1 + \mu_2$ and a fraction $1 - p$ of the bonds have a stretch modulus $\mu_2$. For all $\kappa_1 > 0$, the rigidity threshold is at $p_b \approx 0.442$ [Figs. 6(b) to 6(f)]. We see evidence for a bending to stretching transition at $p_{cf}$ when the bending modulus is small, as a strong decrease of the shear modulus when $p$ drops

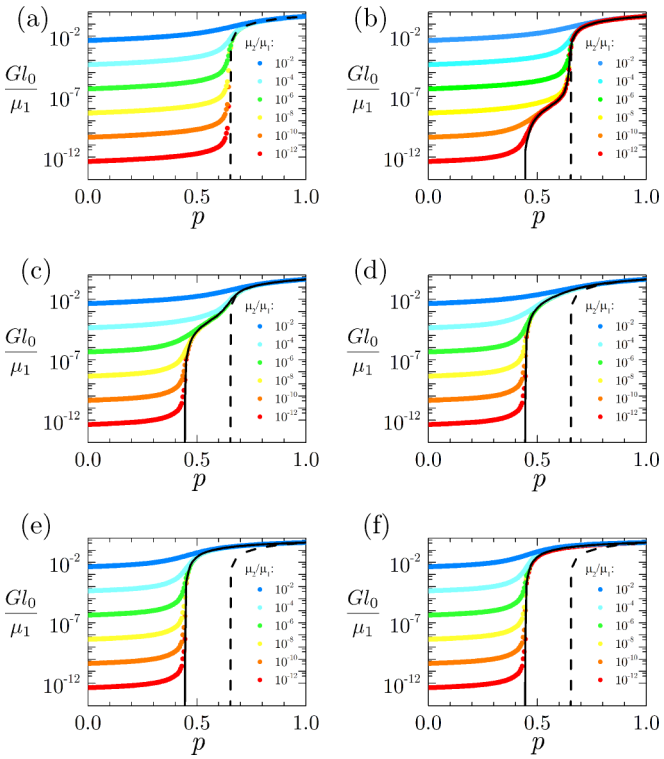


FIG. 6. Elasticity of composite networks for different bending rigidity. Shear modulus $G$ (in units $\mu_1/l_0$) as a function of the bond probability $p$ for a range of stiffnesses of the background matrix for different values of $\kappa_1/\mu_1 l_0^2$: (a) 0, (b) $10^{-8}$, (c) $10^{-4}$, (d) $10^{-2}$, (e) 1, and (f) $10^2$. The black line corresponds to $\mu_2 = 0$ and the dashed line to $\mu_2 = 0$ and $\kappa_1 = 0$. In each figure, the values of $\mu_2/\mu_1$ are (from top to bottom): $10^{-2}$, $10^{-4}$, $10^{-6}$, $10^{-8}$, $10^{-10}$, $10^{-12}$.

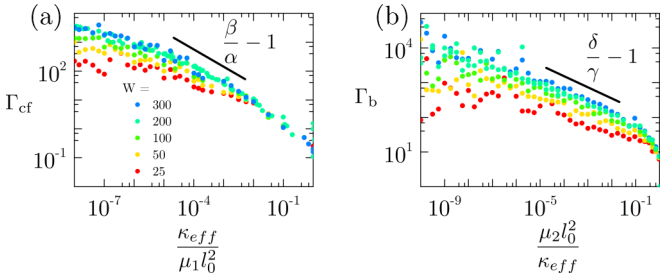


FIG. 7. Nonaffine fluctuations in the two critical regions. (a) Peak in $\Gamma$ at $p = p_{cf}$ as a function of $\kappa_{eff}/\mu_1$, and (b) peak in $\Gamma$ at $p = p_b$ as a function of $\mu_2/\kappa_{eff}$, both for various lattice sizes.

below $p_{cf}$. However, for $\kappa_1/\mu_1 l_0^2 \leqslant 10^{-2}$, bending becomes too costly so that this transition vanishes and the shear modulus is stretching-dominated for all $p > p_b$. The results of Fig. 6 have been used, together with those in Fig. 2, to characterize the different mechanical regimes of composite networks as a function of $p$, $\kappa_1$, and $\mu_2$, as shown in Fig. 3.

## APPENDIX B: MAGNITUDE OF THE NONAFFINE FLUCTUATIONS

As shown in Fig. 4(a), the nonaffine fluctuations show cusp-like peaks a both $p = p_{cf}$ and $p = p_b$. The peak in $\Gamma$ at the central force isostatic point $\Gamma_{cf}$ is due to nonaffine bending fluctuations [Figs. 1(a) and 4(b). These fluctuations are reduced as the effective bending rigidity $\kappa_{eff} = \kappa_1 + \mu_2 l_0^2$ increases. We find that $\Gamma_{cf} \sim (\mu_1/\kappa_{eff})^x$ with $x = 0.53 \approx 1 - \beta/\alpha$ [Fig. 7(a)]. The shear modulus at this point is determined by the bending energy, so that $G_{cf} \sim \kappa_{eff}\Gamma_{cf} \sim \kappa_{eff}^{\beta/\alpha}\mu_1^{1-\beta/\alpha}$. Note that a deviation from the scaling of $\Gamma_{cf}$ is observed for small values of $\kappa_{eff}$, which we attribute to a finite-size effect: the finite size of the lattice limits the maximum size of the collective nonaffine modes. Indeed, we find that $\Gamma_{cf}$ decreases as the lattice size decreases [Fig. 7(a)]. The peak in $\Gamma$ at the bending rigidity threshold, $\Gamma_b$ is determined by rigid rotations of fiber clusters [Figs. 1(b) and 4(c)]. An increase of the matrix stiffness suppresses these modes, so that $\Gamma_b$ decreases as $\mu_2$ increases [Fig. 7(b)]. However, this suppression goes at the cost of increased bending, so that the nonaffine fluctuations at this point are determined by a compromise between matrix stretching and fiber bending. We find that $\Gamma_b \sim (\kappa_{eff}/\mu_2)^y$ with $y = 0.33 \approx 1 - \delta/\gamma$, highlighting the critical state of the network for $\mu_2 \to 0$. The shear modulus at this point is mainly determined by the elastic energy of the matrix, so that $G_b \sim \mu_2\Gamma_b \sim \mu_2^{\delta/\gamma}\kappa_1^{1-\delta/\gamma}$. Again, we observe deviations from the scaling of $\Gamma_b$ for small lattice sizes and small $\mu_2$.

## APPENDIX C: EFFECTIVE BENDING RIGIDITY OF A FIBER IN AN ELASTIC MEDIUM

We consider an elastic rod of length $L$ embedded in an infinite 2D elastic medium. Here, we treat the matrix as a continuous medium with shear modulus $G_2$. A bending deformation of the rod increases the total energy of the

system [27]

$$E = \frac{\kappa_1}{2}\int_0^L \left(\frac{d^2u}{dx^2}\right)^2 dx + \frac{\alpha_2}{2}\int_0^L u^2 dx, \qquad \text{(C1)}$$

where $u(x)$ is the transversal displacement of the rod as a function of the axial coordinate along the rod, and where the parameter $\alpha_2$ represents the effective spring constant of the matrix, which is proportional to the shear modulus $G_2$ as discussed below. The first term represents the bending energy of the rod and the second term represents the elastic energy due to the deformation of the matrix. We assume that the length of the rod does not change upon bending so that we can neglect the stretching energy. We assume a deformation of the form

$$u(x) = u_0 \sin\left(\frac{n\pi x}{L}\right) \quad \text{with } n = 1,2,\ldots. \qquad \text{(C2)}$$

Substitution in Eq. (C1) then gives

$$E = \frac{n^4\pi^4 u_0^2}{4L^3}[\kappa_1 + \alpha_2(L/n\pi)^4]. \qquad \text{(C3)}$$

This can be interpreted as a the energy of a bent rod with an effective bending rigidity $\kappa_{\text{eff}} = \kappa_1 + \alpha_2(L/n\pi)^4$.

While for a three-dimensional medium, the effective spring constant is related to the shear modulus of the medium as $\alpha_2 \approx 4\pi G_2/\ln(L/d)$ with $a$ the diameter of the rod [27], for a 2D medium we can derive [33] $\alpha_2 \approx 4\pi G_2/L$. Since the shear modulus of a triangular spring network is equal to $G_2 = \frac{1}{4}\sqrt{3}\mu_2/l_0$, we finally find

$$\kappa_{\text{eff}} = \kappa_1 + A\mu_2 l_0^2 \qquad \text{(C4)}$$

with $A = \frac{\sqrt{3}}{n^4\pi^3}(L/l_0)^3$. The prefactor $A$ depends on the rod length $L$ and on the mode number $n$. Around the central force isostatic point, the average fiber length is $L = l_0/(1 - p_{\text{cf}}) \approx 2.8l_0$. Assuming that the dominant bending mode is the lowest energy mode, $n = 1$, we find $A \approx 1.3$, close to the value of unity used to collapse the data in Fig. 3.


[1] C. P. Broedersz and F. C. MacKintosh, Modeling semiflexible polymer networks, Rev. Mod. Phys. **86**, 995 (2014).

[2] J. Wilhelm and E. Frey, Elasticity of Stiff Polymer Networks, Phys. Rev. Lett. **91**, 108103 (2003).

[3] D. A. Head, A. J. Levine, and F. C. MacKintosh, Deformation of Cross-Linked Semiflexible Polymer Networks, Phys. Rev. Lett. **91**, 108102 (2003).

[4] D. A. Head, A. J. Levine and F. C. MacKintosh, Distinct regimes of elastic response and deformation modes of cross-linked cytoskeletal and semiflexible polymer networks, Phys. Rev. E **68**, 061907 (2003).

[5] M. Das, F. C. MacKintosh and A. J. Levine, Effective Medium Theory of Semiflexible Filamentous Networks, Phys. Rev. Lett. **99**, 038101 (2007).

[6] C. P. Broedersz, X. Mao, T. C. Lubensky, and F. C. MacKintosh, Criticality and isostaticity in fibre networks, Nat. Phys. **7**, 983 (2011).

[7] M. Gardel *et al.*, Elastic behavior of cross-linked and bundled actin networks, Science **304**, 1301 (2004).

[8] O. Lieleg, M. M. A. E. Claessens, C. Heussinger, E. Frey, and A. R. Bausch, Mechanics of Bundled Semiflexible Polymer Networks, Phys. Rev. Lett. **99**, 088102 (2007).

[9] A. Sharma *et al.*, Strain-controlled criticality governs the nonlinear mechanics of fibre networks, Nat. Phys. **12**, 584 (2016).

[10] A. Bausch and K. Kroy, A bottom-up approach to cell mechanics, Nat. Phys. **2**, 231 (2006).

[11] U. Wegst and M. Ashby, The mechanical efficiency of natural materials, Philos. Mag. **84**, 2167 (2004).

[12] E. Munch *et al.*, Tough, bio-inspired hybrid materials, Science **322**, 1516 (2008).

[13] U. G. K. Wegst, H. Bai, E. Saiz, A. P. Tomsia, and R. O. Ritchie, Bioinspired structural materials, Nat. Mater. **14**, 23 (2015).

[14] K.-I. Jang *et al.*, Soft network composite materials with deterministic and bio-inspired designs, Nat. Commun. **6**, 6566 (2015).

[15] J. Gong, Y. Katsuyama, T. Kurokawa, and Y. Osada, Double-network hydrogels with extremely high mechanical strength, Adv. Mater. **15**, 1155 (2003).

[16] J.-Y. Sun *et al.*, Highly stretchable and tough hydrogels, Nature (London) **489**, 133 (2012).

[17] W. H. Rombouts, M. Giesbers, J. van Lent, F. A. de Wolf, and J. van der Gucht, Synergistic stiffening in double-fiber networks, Biomacromolecules **15**, 1233 (2014).

[18] W. H. Rombouts, M. Colomb-Delsuc, M. W. T.. Werten, S. Otto, F. A. de Wolf, and J. van der Gucht, Enhanced rigidity and rupture strength of composite hydrogel networks of bio-inspired block copolymers, Soft Matter **9**, 6936 (2013).

[19] E. M. Huisman, C. Heussinger, C. Storm, and G. T. Barkema, Semiflexible Filamentous Composites, Phys. Rev. Lett. **105**, 118101 (2010).

[20] M. Bai, A. R. Missel, W. S. Klug, and A. J. Levine, The mechanics and affine-nonaffine transition in polydisperse semiflexible networks, Soft Matter **7**, 907 (2011).

[21] L. Zhang, S. P. Lake, V. H. Barocas, M. S. Shephard, and R. C. Picu, Cross-linked fiber network embedded in an elastic matrix, Soft Matter **9**, 6398 (2013).

[22] H. Wada and Y. Tanaka, Mechanics and size-dependent elasticity of composite networks, Europhys. Lett. **87**, 58001 (2009).

[23] M. Das and F. C. MacKintosh, Mechanics of soft composites of rods in elastic gels, Phys. Rev. E **84**, 061906 (2011).

[24] A. S. Shahsavari and R. C. Picu, Exceptional stiffening in composite fiber networks, Phys. Rev. E **92**, 012401 (2015).

[25] J. C. Maxwell, On the calculation of the equilibrium and stiffness of frames, Philos. Mag. **27**, 294 (1864).

[26] X. Mao, O. Stenull, and T. C. Lubensky, Effective-medium theory of a filamentous triangular lattice, Phys. Rev. E **87**, 042601 (2013).

[27] C. Brangwynne *et al.*, Microtubules can bear enhanced compressive loads in living cells because of lateral reinforcement, J. Cell Biol. **173**, 733 (2006).

[28] M. Sahimi and S. Arbabi, Mechanics of disordered solids. II. Percolation on elastic networks with bond-bending forces, Phys. Rev. B **47**, 703 (1993).

[29] E. J. Garboczi and M. F. Thorpe, Effective-medium theory of percolation on central-force elastic networks. III. The superelastic problem, Phys. Rev. B **33**, 3289 (1986).

[30] B. DiDonna and T. Lubensky, Nonaffine correlations in random elastic media, Phys. Rev. E **72**, 066619 (2005).

[31] C. Heussinger and E. Frey, Floppy Modes and Nonaffine Deformations in Random Fiber Networks, Phys. Rev. Lett. **97**, 105501 (2006).

[32] P. R. Onck, T. Koeman, T. van Dillen, and E. van der Giessen, Alternative Explanation of Stiffening in Cross-Linked Semiflexible Networks, Phys. Rev. Lett. **95**, 178102 (2005).

[33] A. J. Levine, T. B. Liverpool, and F. C. MacKintosh, Dynamics of Rigid and Flexible Extended Bodies in Viscous Films and Membranes, Phys. Rev. Lett. **93**, 038102 (2004).